Programmable Quantum Simulations on a Trapped-Ion Quantum Computer with a Global Drive

Yotam Shapira,[1,*] Jovan Markov,[1,*] Nitzan Akerman,[1] Ady Stern,[2] and Roee Ozeri[1]
[1]Department of Physics of Complex Systems, Weizmann Institute of Science, Rehovot 7610001, Israel
[2]Department of Physics of Condensed Matter Systems, Weizmann Institute of Science, Rehovot 7610001, Israel

(Received 21 December 2023; accepted 4 December 2024; published 6 January 2025)

Simulation of quantum systems is notoriously challenging for classical computers, while quantum hardware is naturally well-suited for this task. However, the imperfections of contemporary quantum systems pose a considerable challenge in carrying out accurate simulations over long evolution times. Here, we experimentally demonstrate a method for quantum simulations on a small-scale trapped-ion–based quantum simulator. Our method enables quantum simulations of programmable spin-Hamiltonians, using only simple global fields, driving all qubits homogeneously and simultaneously. We measure the evolution of a quantum Ising ring and accurately reconstruct the Hamiltonian parameters, showcasing an accurate and high-fidelity simulation. Our method enables a significant reduction in the required control and depth of quantum simulations, thus generating longer evolution times with higher accuracy.

DOI: 10.1103/PhysRevLett.134.010602

Quantum simulators are controllable quantum systems that enable the study of phases, dynamics, and properties of complex quantum systems for which an analytical or numerical treatment is challenging [1]. Quantum simulations are considered a suitable task for noisy intermediate scale quantum (NISQ) computers [2], which are currently available. Recent years have seen numerous implementations of quantum simulations on several platforms [3–5], which are performed with an ever-increasing quality, approaching an advantage over classical methods. An apparent challenge to NISQ-era quantum hardware is to perform large-scale quantum simulations, with a relatively shallow circuit depth, i.e., with few operations, in order to avoid the deterioration of the simulation's fidelity due to noise.

Ion crystals trapped in radio frequency traps are an especially prolific tool for quantum simulations [6–19] due to their long coherence times [20,21], high-fidelity control [22–25], and rich connectivity [26–29]. By exploiting the long-range coupling between all ions in the ion crystal, it is possible to perform parallel and long-range entanglement, potentially increasing the efficacy of the simulation. Analog quantum simulation in trapped-ion platforms are typically either limited to simple models that are constrained by the one-dimensional (1D) structure of the underlying ion crystal [15] or require local control [18].

Here, we experimentally implement quantum simulations of the Ising-spin model on a small-scale trapped-ion quantum system [30]. We evolve our system using global pulses, which drive the ions homogeneously and nevertheless generate a desired inhomogeneous programmable interaction in each pulse, which is unconstrained by the 1D linear geometry of the ion chain. This is enabled by coherently and simultaneously coupling to all modes of motion of the trapped-ion crystal in a controllable manner. We are able to simulate spin-Hamiltonians of the form

$$H = \sum_{n,m=1}^{N} J_{n,m}\sigma_x^{(n)}\sigma_x^{(m)}, \tag{1}$$

with $\sigma_x^{(n)}$ a Pauli-x operator acting on the nth spin of a N site spin system, and $J_{n,m}$ an experimentally controllable coupling matrix. This implements an Ising-spin model.

With global methods that are straightforward in trapped-ion systems, we extend this interaction to accommodate for a transverse field, $\delta\sum_{n=1}^{N}\sigma_z^{(n)}$. Similarly, we can add $\sigma_y^{(n)}\sigma_y^{(m)}$ terms that may differ in their coupling matrix compared to the coupling in Eq. (1).

Our method takes into account and mitigates unwanted inhomogeneous aberrations due to, e.g., a finite driving beam waist. Furthermore, while all modes of motion of the ion crystal may be used, here we explicitly decouple from the center-of-mass mode as it is more prone to heating and decoherence, without affecting our method's programmability, thus improving the simulation's fidelity.

We simulate a four-ion Ising-spin quantum ring and observe dynamics under its Hamiltonian. We supplement this model with a transverse field, such that the resulting evolution is purely quantum mechanical, and observe the dynamics as a function of the transverse field magnitude.

*These authors contributed equally to this work.

Below we analyze these results in full and are able to accurately reconstruct both the Ising coupling terms, $J_{n,m}$, as well as the various transverse fields, δ, showcasing an accurate realization of quantum simulations using our method.

The theoretical proposal underpinning our Letter has been proposed in Refs. [26,27]. We provide the relevant physical picture and method details. In trapped-ion–based quantum systems, entanglement between qubits is typically generated by spin-dependent forces, which mediate spin-spin interactions through the collective phonon modes of motion of the ion crystal. Conventionally only two ions are driven and coupled to a single phonon mode, such as in the Mølmer-Sørensen (MS) gate [31,32], generating an evolution of the form $U_{\mathrm{MS}} = \exp(i\Phi\sigma_x^{(n)}\sigma_x^{(m)})$, with n and m the indices of the two entangled ions and Φ a controllable entanglement phase.

This method is generalized by homogeneously driving all of the N ions in the ion crystal. We purposefully couple to N modes of motion along the axial axis of the ion crystal. As shown in Ref. [26], at a fixed pulse duration, such a drive yields the evolution

$$U = \exp\left(i \sum_{j=1}^{N} \Phi_j \sum_{n,m=1}^{N} O_j^{(n)} O_j^{(m)} \sigma_x^{(n)} \sigma_x^{(m)} \right), \qquad (2)$$

with the $\{\Phi_j\}_{j=1}^N$ completely controllable mode-dependent entanglement phase, and O an orthonormal mode matrix, i.e., $O_j^{(n)}$ is the normalized participation of the nth ion in the jth mode of motion [33].

We drive the ions in the adiabatic regime, i.e., the pulse duration implementing U is slower than the characteristic oscillation periods of the modes of motions. In this regime the mapping between the set of desired phases, $\{\Phi_j\}_{j=1}^N$, and the details of the drive is straightforward, as described below. Faster realizations of U are discussed in Ref. [27].

Our drive is composed of four tones per motional mode: $\omega_{j,1,\pm} = \omega_0 \pm (\nu_j + \xi)$ and $\omega_{j,3,\pm} = \omega_0 \pm (\nu_j + 3\xi)$, with ν_j the frequency of the jth mode of motion and ω_0 the single-qubit transition frequency. ξ is an additional detuning from the mode transition frequencies such that U in Eq. (2) is achieved at $t = 2\pi/\xi$.

The phases of the tones of $\omega_{j,1,\pm}$ are set to 0 (for all j's) and the phases of the tones $\omega_{j,3,\pm}$ are set to π. With these choices the resulting evolution is made robust to unwanted coupling to the carrier transition and pulse-timing errors [26,34,35].

The amplitudes of $\omega_{j,n,\pm}$, driving the jth mode of motion are set to r_j. With these generalizations of the MS gate we make use of consecutive implementations of U in Eq. (2), such that the ion's evolution, at integer multiples of $2\pi/\xi$, evolves stroboscopically according to the Hamiltonian in Eq. (1), and $J_{n,m} \propto \sum_{j=1}^{N} (\eta_j^2 r_j^2/\xi) O_j^{(n)} O_j^{(m)}$, with η_j the Lamb-Dicke parameter of the jth mode of motion. The proportionality constant accommodates for the laser's total Rabi frequency, Ω_0, and additional (mode and ion independent) numerical factors.

Because of the orthonormality of O, shifting all Φ_j's by a constant, i.e., $\Phi_j \mapsto \Phi_j + \phi$, amounts to modifying U in Eq. (2) by a global phase, i.e., $U \mapsto e^{iN\phi}U$ [36]. Here, we exploit this property in order to set $\Phi_{j=1} = 0$, and adjust all the other Φ_j's appropriately. This is helpful as the $j = 1$ mode is an axial center-of-mass mode, which typically exhibits the fastest heating and decoherence rate. Thus, we decouple from this mode, yielding longer coherence times and higher simulation fidelity.

Furthermore, inhomogeneities in the field driving the ions, e.g., due to a finite beam waist of an optical drive, can be taken into account by adjusting O accordingly [36], enabling mitigation of such effects.

The Pauli-x rotations, i.e., $\sigma_x^{(n)}$, in Eq. (2) can be trivially generalized to $\sigma_\phi^{(n)} = \cos(\phi)\sigma_x^{(n)} + \sin(\phi)\sigma_y^{(n)}$, with ϕ fully controllable, by equally shifting the phases of the drive's tones. The choice of ϕ, as well as all other drive parameters such as the different Φ_j's, can be changed at each consecutive implementation of U. Combined with the well-known Suzuki-Trotter decomposition [37,38], this accommodates for various spin-Hamiltonians, e.g.,

$$H = \sum_{n,m=1}^{N} \left[J_{n,m}^{(x)} \sigma_x^{(n)} \sigma_x^{(m)} + J_{n,m}^{(y)} \sigma_y^{(n)} \sigma_y^{(m)} \right] + \delta \sum_{n=1}^{N} \sigma_z^{(n)}, \qquad (3)$$

with $J_{n,m}^{(x)}$ and $J_{n,m}^{(y)}$ controllable couplings and δ a controllable transverse field. The $\sigma_y^{(n)}$ terms are generated by a $\pi/2$ jump in ϕ, while the transverse $\sigma_z^{(n)}$ terms are generated by a gradual linear ramp of ϕ in each consecutive Suzuki-Trotter block.

The general Hamiltonian in Eq. (3), as well as more elaborate time-dependent Hamiltonians, are all made possible while still using a global driving field. We remark that H commutes with the parity operator $P = \exp(i\pi \sum_{n=1}^{N} \sigma_z^{(n)})$, thus states with well-defined parity, e.g., superpositions of states with an even number of spin excitations, will remain with the same parity throughout their evolution.

We experimentally implement quantum simulations on a small-scale trapped-ion quantum simulator [30], in which the $|5S_{\frac{1}{2},\frac{1}{2}}\rangle$ ($|4D_{\frac{5}{2},\frac{3}{2}}\rangle$) states of $^{88}Sr^+$ ions are mapped to $|0\rangle$ ($|1\rangle$) qubit levels. These levels are coupled, using a quadrupole transition, by a 674 nm narrow linewidth laser [39], illuminating the ions approximately homogeneously with a wide global beam. We modulate the 674 nm beam appropriately such that it has a rich spectrum, containing M frequency pairs, $\{\omega_0 \pm \omega_m\}_{m=1}^M$, with appropriate amplitudes and phases, as prescribed above.

We first investigate dynamics under a four-site spin ring, with antiperiodic boundary conditions, i.e., the nearest-neighbor (NN) Hamiltonian,

$$H_{\mathrm{ring,ap}} = \Omega\left(\sigma_x^{(1)}\sigma_x^{(2)} + \sigma_x^{(2)}\sigma_x^{(3)} + \sigma_x^{(3)}\sigma_x^{(4)} - \sigma_x^{(4)}\sigma_x^{(1)}\right) + \delta\sum_{n=1}^{4}\sigma_z^{(n)}, \tag{4}$$

with "antiperiodicity" (ap) manifested as the negative sign of the $\sigma_x^{(4)}\sigma_x^{(1)}$ coupling term.

This Hamiltonian is analytically solvable, and thus we use it as a proof of concept for highlighting key components of our method—namely, freely generating positive and negative coupling terms, long-range terms that are not restricted by the 1D underlying ion crystal, and correction of aberrations due to finite beam width. Furthermore, it is physically motivated, since with a Jordan-Wigner [40] transformation the system is mapped to an even number of fermions hopping on a periodic ring (with no negative couplings) [41,42].

$H_{\mathrm{ring,ap}}$ can be well-approximated by the axial modes of motion of our harmonic ion trap. The method for choosing the appropriate entanglement phases is detailed in [26,36], yielding, $\mathbf{\Phi}^{(\mathrm{optimal})} = (0, 0.3867, -0.7071, -1.0939)$, with an ideal implementation fidelity of $H_{\mathrm{ring,ap}}$ of 0.989 (defined precisely below). We note that Ref. [43] provides a systematic analysis of the possible couplings schemes enabled by global modes and that Refs. [44,45] further expand these possibilities by directly shaping the global mode structure.

We first benchmark our simulation with $\delta = 0$. To do so we initialize the system to the ground state, $|0000\rangle$, evolve it under $H_{\mathrm{ring,ap}}$, and measure the population at the different spin states. Figure 1 shows the state occupations after such an evolution, with the spin populations grouped in terms of their respective excitation subspaces (ESs), i.e., the number of excitations in each state. The evolution is sampled stroboscopically, at integer multiples of U, yielding data (points) with error bars that reflect $\pm 2\sigma$ statistical errors due to quantum projection noise. Here and in the measurements below we use $\xi = 5$ kHz. Since the initial state is the ground state we expect the evolution to remain in even subspaces 0ES (green), 2ES (orange), and 4ES (blue). Thus we postselect and normalize to the population in even subspaces.

The data are shown together with the ideal theoretical prediction of the evolution under $H_{\mathrm{ring,ap}}$ (dashed lines). As previously analyzed in Ref. [7], discrepancies between the data and theoretical prediction are attributed to qubit dephasing ($T_2 \approx 5$ ms). We account for it, as well as inaccuracies of the $J_{n,m}$'s, using a Lindblad master equation, and use it to fit the six independent parameters of $J_{n,m}$ and T_2. The fit matches the populations measured over all

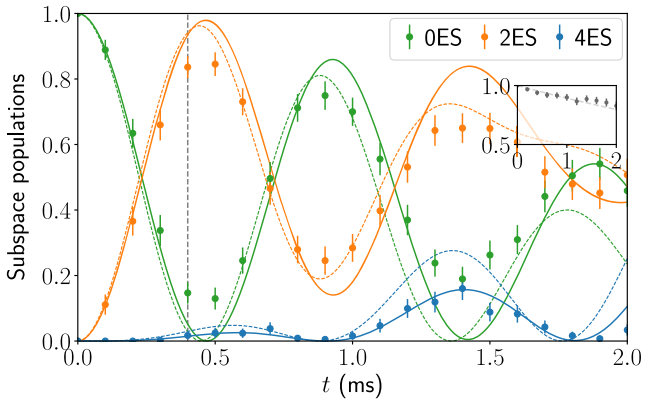

FIG. 1. Excitation subspace dynamics of the antiperiodic Ising-spin ring. Populations are measured at consecutive implementations of U (points), and grouped into excitation subspaces (colors). The theoretical prediction (dashed) shows a good agreement with the data. A more involved model that includes dephasing (solid) is fitted to the data yielding a mean fit error of < 0.0155. Populations in the even excitation subspaces (green, orange, and blue) exhibit coherent oscillations. The inset shows the total (unnormalized) population in the even subspaces (points), which slowly decreases due to decoherence and is well fitted by our full model (dashed).

eight even-excitation states, with an average population error of < 0.0155 per state per data point, which is consistent with shot-noise errors under 500 experimental repetitions per point, and a characteristic coupling rate of $\tilde{\Omega} \approx 1.13$ kHz (further details in [36]).

Furthermore, this analysis predicts population "leakage" from the even excitation subspaces (inset of Fig. 1), as well as deviations between the ideal and measured evolution, all of which are accounted for by qubit dephasing. Thus improving T_2 will enable longer simulations with greater fidelity.

Various methods exist to validate the performance of our simulation [46–48]. Here, we directly benchmark our simulation by performing parity measurements. Such a method has been recently employed in Ref. [49]. We do so by evolving the system for a short time, $t_{\mathrm{cor}} = 400$ μs (vertical dashed gray in Fig. 1), corresponding to two consecutive implementations of U, and then applying a global "analysis" $\pi/2$ pulse with phase ϕ. That is, the system evolves according to

$$U_{\mathrm{cor}} = e^{\frac{i\pi}{22}\sum_{n=1}^{N}\sigma_\phi^{(n)}} e^{i\Omega t_{\mathrm{cor}}\sum_{n,m}J_{n,m}\sigma_x^{(n)}\sigma_x^{(m)}}, \tag{5}$$

after which we measure state occupations and evaluate the bipartite correlations, $\langle\sigma_z^{(n)}\sigma_z^{(m)}\rangle$. This process constitutes a measurement of $C_{n,m}(\phi) = \langle\psi(t)|\sigma_{\phi'}^{(n)}\sigma_{\phi'}^{(m)}|\psi(t)\rangle$, with $\phi' = \phi - \pi/2$ and $|\psi(t)\rangle = U(t)|0000\rangle$. For short evolution

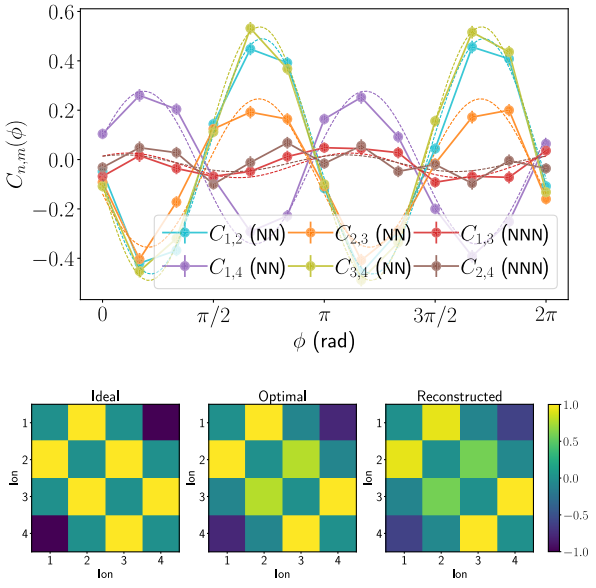

FIG. 2. Top: the correlation $C_{n,m} = \langle \sigma_\phi^{(n)} \sigma_\phi^{(m)} \rangle$ is evaluated for pair of sites, at various values of ϕ, after a small evolution time $t_{\text{parity}} = 4\pi\xi^{-1}$. We observe high-contrast oscillations between sites that are NN. The antiperiodic coupling of $\sigma_x^{(1)}\sigma_x^{(4)}$ in Eq. (4) is manifested as an opposite-phase fringe of $C_{1,4}$ (purple). Error bars reflect $\pm 2\sigma$ statistical errors due to quantum projection noise. Data (points) are fitted to a single oscillating sine (dashed) showing a good fit. Bottom: coupling matrices, $J_{n,m}$, of the antiperiodic Ising-spin ring. Showing ideal values (left) read off the model's Hamiltonian in Eq. (4), optimal values (middle) due to a global drive implementation, and reconstructed values (right), using the parity fits (top). The matrices are normalized such that the largest entry in each of them is 1 (arbitrary units).

times, $\Omega t_{\text{cor}} J_{n,m} \ll 1$, we get $C_{n,m} = -2\Omega t_{\text{cor}} J_{n,m} \sin(2\phi)$ with corrections that are cubic in Ωt_{cor} [36].

The results of these measurements, for various rotation phases ϕ, are shown in Fig. 2 (top). We observe that correlations that are NN on the spin-ring (cyan, orange, olive, and purple) exhibit high-contrast fringes, while next-to-nearest-neighbor (NNN) sites (red and brown) do not. Because of the antiperiodic boundary conditions, $C_{1,4}$ (purple) exhibits an oscillation phase that is opposite to all other pairs. Variations of the global drive on the ions may reduce the fidelity of the analysis pulse and bias our data. However, this effect is quadratic in the field inhomogeneity [36], and may be further mitigated with well-known amplitude-robust composite pulses. Here, we simply rescale the fringe contrasts, using the relative local Rabi frequencies in the ion crystal, constituting a $< 1\%$ effect to the data.

We fit each correlation fringe to a sine function with frequency 2ϕ (dashed), yielding a mean fitting error of 0.018, well within error bars. The resulting fitted amplitudes, $J_{n,m}^{\text{reconstructed}}$, are presented in Fig. 2 (bottom, right), along with the ideal values of $J_{n,m}^{\text{ideal}}$ (bottom, left), which are directly read off the model's Hamiltonian in Eq. (4), as well as the expected values of the implemented model, $J_{n,m}^{\text{optimal}}$ (bottom, middle), originating from our choice $\mathbf{\Phi}^{(\text{optimal})}$, and the system's modes of motion [33,36] (middle).

To quantify our reconstruction, we consider the Cartesian overlap of the nontrivial values of the various J's. Specifically we define $F(J_1, J_2) \equiv \boldsymbol{J}_1 \cdot \boldsymbol{J}_2 / \sqrt{(\boldsymbol{J}_1 \cdot \boldsymbol{J}_1)(\boldsymbol{J}_2 \cdot \boldsymbol{J}_2)}$, with $\boldsymbol{J}_1$, $\boldsymbol{J}_2$ being six-element real vectors constructed from the upper triangular entries of the coupling matrices J_1 and J_2 (excluding the trivial diagonal). This metric corresponds to the Hilbert-Schmidt (HS) fidelity between Hamiltonians, $F_{\text{HS}}(H_1, H_2) = |\text{Tr}(H_1 H_2)| / \sqrt{\text{Tr}(H_1^2)\text{Tr}(H_2^2)}$, when considering Hamiltonians constructed by $\sigma_x^{(n)}\sigma_x^{(m)}$-type interactions, which is natural in our setup. The denominator makes the comparison relative, i.e., up to a rate factor, Ω.

The three reconstructed coupling matrices are in good agreement. Indeed the overlap yields $F(J^{\text{ideal}}, J^{\text{optimal}}) = 0.989$ and $F(J^{\text{optimal}}, J^{\text{reconstructed}}) = 0.993^{-0.042}_{+0.007}$, indeed verifying a high-quality implementation of the intended ring model. These high-fidelity results may seem contradictory to measured dynamics in Fig. 1, where the ideal (dashed) values deviate significantly from the data (points) or fit (solid). However, this is simply a manifestation of the well-known robustness of correlation measurements to uncorrelated noise [50–52].

We now turn to study the effects of the transverse field, δ, in the ring Hamiltonian in Eq. (4). This term generates a global σ_z coupling that does not commute with the Ising NN interaction. At high transverse field value, i.e., $\delta/\tilde{\Omega} \gg 1$ the initial state, $|0000\rangle$ becomes an eigenstate. Thus, approaching this limit, we expect an effective slowing down of the observed dynamics.

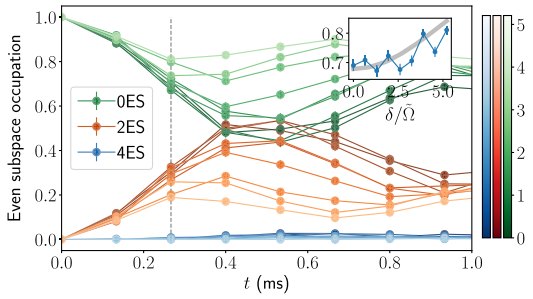

FIG. 3. Dynamics of an antiperiodic Ising-spin ring, with a transverse field. We evolve the state $|0000\rangle$ under the system's Hamiltonian. Populations (points) are grouped according to their ES (legend), and postselected to even subspaces. We repeat this measurement for various magnitudes of transverse fields, $\delta/\tilde{\Omega}$ (color bars). For $\delta \gg \tilde{\Omega}$ the initial state becomes an eigenstate, leading to a suppression of dynamics. Error bars reflect 2σ errors due to quantum projection noise. Inset: measured ground state population (blue) after a short evolution time, $t = 4\pi\xi^{-1}$ (vertical, gray), compared to an exact simulation (gray), showing good agreement.

Figure 3 shows the postselected populations in even excitation subspaces (points connected by lines) for various choices of $\delta/\tilde{\Omega}$ (color bars). Indeed, the ground state (green lines) remains more populated throughout the observed dynamics for larger values (brighter) of $\delta/\tilde{\Omega}$, while two excitations (orange) and four excitations (blue) become less frequent.

To analyze the data further, and benchmark our simulation, we consider the population in the ground state, Pr (0000), after two consecutive applications of U in Eq. (2) and the transverse field term (dashed gray line). Since δ acts to detune the NN interaction, similar to off-resonance Rabi oscillations, we expect a quadratic suppression of dynamics. Indeed, the inset of Fig. 3 shows the measured ground state population (blue), which exhibits a quadratic increase as a function of δ. We also plot the theoretical prediction by directly simulating the Hamiltonian in Eq. (4) (gray) showing a qualitative correspondence. We remark that for large values of δ the Trotter approximation becomes less accurate, which may account for the discrepancy between data and theory at $\delta/\tilde{\Omega} \approx 5$.

In conclusion, we have demonstrated a method for programmable quantum simulations of spin-Hamiltonians on trapped-ion chains. The method, based on the proposal in Ref. [26], can be used to generate a variety of models and coupling geometries, which are unconstrained by the physical realization of the 1D linear ion crystal. Here, we employ it to generate a four-site antiperiodic Ising-spin ring. We use population and correlation data in order to benchmark our simulation. Indeed we reconstruct the applied couplings and transverse field, showing a faithful generation of the intended model. This method is well-suited for NISQ-era quantum systems as it can be used to leverage typical shallow circuits yet still generate long evolution times of relevant quantum systems.

Note added—We recently became aware of similar works by Wu *et al.* [16] and Lu *et al.* [17], which use similar techniques in order to implement similar Ising models.

Acknowledgments—This work was supported by the Israeli Science Foundation, the Israeli Ministry of Science Technology and Space, the Minerva Stiftung, the European Union's Horizon 2020 research and innovation programme (Grant Agreement LEGOTOP No. 788715), the DFG (CRC/Transregio 183, EI 519/7-1), and ISF Quantum Science and Technology (2074/19).

[1] R. P. Feynman, Simulating physics with computers, Int. J. Theor. Phys. **21**, 467 (1982).
[2] J. Preskill, Quantum computing in the NISQ era and beyond, Quantum **2**, 79 (2018).
[3] C. Neill *et al.*, Accurately computing the electronic properties of a quantum ring, Nature (London) **594**, 508 (2021).
[4] Y. Kim, A. Eddins, S. Anand, K. X. Wei, E. van den Berg, S. Rosenblatt, H. Nayfeh, Y. Wu, M. Zaletel, K. Temme, and A. Kandala, Evidence for the utility of quantum computing before fault tolerance, Nature (London) **618**, 500 (2023).
[5] G. Semeghini, H. Levine, A. Keesling, S. Ebadi, T. T. Wang, D. Bluvstein, R. Verresen, H. Pichler, M. Kalinowski, R. Samajdar, A. Omran, S. Sachdev, A. Vishwanath, M. Greiner, V. Vuletić, and M. D. Lukin, Probing topological spin liquids on a programmable quantum simulator, Science **374**, 1242 (2021).
[6] T. Manovitz, Y. Shapira, N. Akerman, A. Stern, and R. Ozeri, Quantum simulations with complex geometries and synthetic gauge fields in a trapped ion chain, PRX Quantum **1**, 020303 (2020).
[7] Y. Shapira, T. Manovitz, N. Akerman, A. Stern, and R. Ozeri, Quantum simulations of interacting systems with broken time-reversal symmetry, Phys. Rev. X **13**, 021021 (2023).
[8] C. Kokail, C. Maier, R. van Bijnen, T. Brydges, M. K. Joshi, P. Jurcevic, C. A. Muschik, P. Silvi, R. Blatt, C. F. Roos *et al.*, Self-verifying variational quantum simulation of lattice models, Nature (London) **569**, 355 (2019).
[9] M. K. Joshi, F. Kranzl, A. Schuckert, I. Lovas, C. Maier, R. Blatt, M. Knap, and C. F. Roos, Observing emergent hydrodynamics in a long-range quantum magnet, Science **376**, 720 (2022).
[10] W. L. Tan, P. Becker, F. Liu, G. Pagano, K. S. Collins, A. De, L. Feng, H. B. Kaplan, A. Kyprianidis, R. Lundgren, W. Morong, S. Whitsitt, A. V. Gorshkov, and C. Monroe, Domain-wall confinement and dynamics in a quantum simulator, Nat. Phys. **17**, 742 (2021).
[11] A. Kyprianidis, F. Machado, W. Morong, P. Becker, K. S. Collins, D. V. Else, L. Feng, P. W. Hess, C. Nayak, G. Pagano *et al.*, Observation of a prethermal discrete time crystal, Science **372**, 1192 (2021).
[12] C. Monroe, W. C. Campbell, L.-M. Duan, Z.-X. Gong, A. V. Gorshkov, P. W. Hess, R. Islam, K. Kim, N. M. Linke, G. Pagano, P. Richerme, C. Senko, and N. Y. Yao, Programmable quantum simulations of spin systems with trapped ions, Rev. Mod. Phys. **93**, 025001 (2021).
[13] M. Qiao, Z. Cai, Y. Wang, B. Du, N. Jin, W. Chen, P. Wang, C. Luan, E. Gao, X. Sun, H. Tian, J. Zhang, and K. Kim, Observing frustrated quantum magnetism in two-dimensional ion crystals, arXiv:2204.07283.
[14] M. Iqbal, N. Tantivasadakarn, R. Verresen, S. L. Campbell, J. M. Dreiling, C. Figgatt, J. P. Gaebler, J. Johansen, M. Mills, S. A. Moses, J. M. Pino, A. Ransford, M. Rowe, P. Siegfried, R. P. Stutz, M. Foss-Feig, A. Vishwanath, and H. Dreyer, Non-Abelian topological order and anyons on a trapped-ion processor, Nature (London) **626**, 505 (2024).
[15] D. Porras and J. I. Cirac, Effective quantum spin systems with trapped ions, Phys. Rev. Lett. **92**, 207901 (2004).
[16] Q. Wu, Y. Shi, and J. Zhang, Qubits on programmable geometries with a trapped-ion quantum processor, arXiv:2308.10179.
[17] Y. Lu, W. Chen, S. Zhang, K. Zhang, J. Zhang, J.-N. Zhang, and K. Kim, Realization of programmable Ising models in a trapped-ion quantum simulator, arXiv:2311.04864.

[18] D. Hayes, S. T. Flammia, and M. J. Biercuk, Programmable quantum simulation by dynamic Hamiltonian engineering, New J. Phys. **16**, 083027 (2014).
[19] O. Katz, L. Feng, D. Porras, and C. Monroe, Observing topological insulator phases with a programmable quantum simulator, arXiv:2401.10362.
[20] Y. Wang, M. Um, J. Zhang, S. An, M. Lyu, J.-N. Zhang, L.-M. Duan, D. Yum, and K. Kim, Single-qubit quantum memory exceeding ten-minute coherence time, Nat. Photonics **11**, 646 (2017).
[21] P. Wang, C.-Y. Luan, M. Qiao, M. Um, J. Zhang, Y. Wang, X. Yuan, M. Gu, J. Zhang, and K. Kim, Single ion qubit with estimated coherence time exceeding one hour, Nat. Commun. **12**, 233 (2021).
[22] J. P. Gaebler, T. R. Tan, Y. Lin, Y. Wan, R. Bowler, A. C. Keith, S. Glancy, K. Coakley, E. Knill, D. Leibfried, and D. J. Wineland, High-fidelity universal gate set for $^{9}Be^{+}$ ion qubits, Phys. Rev. Lett. **117**, 060505 (2016).
[23] C. R. Clark, H. N. Tinkey, B. C. Sawyer, A. M. Meier, K. A. Burkhardt, C. M. Seck, C. M. Shappert, N. D. Guise, C. E. Volin, S. D. Fallek, H. T. Hayden, W. G. Rellergert, and K. R. Brown, High-fidelity bell-state preparation with $^{40}Ca^{+}$ optical qubits, Phys. Rev. Lett. **127**, 130505 (2021).
[24] C. J. Ballance, T. P. Harty, N. M. Linke, M. A. Sepiol, and D. M. Lucas, High-fidelity quantum logic gates using trapped-ion hyperfine qubits, Phys. Rev. Lett. **117**, 060504 (2016).
[25] R. Srinivas, S. C. Burd, H. M. Knaack, R. T. Sutherland, A. Kwiatkowski, S. Glancy, E. Knill, D. J. Wineland, D. Leibfried, A. C. Wilson, D. T. C. Allcock, and D. H. Slichter, High-fidelity laser-free universal control of trapped ion qubits, Nature (London) **597**, 209 (2021).
[26] Y. Shapira, R. Shaniv, T. Manovitz, N. Akerman, L. Peleg, L. Gazit, R. Ozeri, and A. Stern, Theory of robust multiqubit nonadiabatic gates for trapped ions, Phys. Rev. A **101**, 032330 (2020).
[27] Y. Shapira, L. Peleg, D. Schwerdt, J. Nemirovsky, N. Akerman, A. Stern, A. B. Kish, and R. Ozeri, Fast design and scaling of multi-qubit gates in large-scale trapped-ion quantum computers, arXiv:2307.09566.
[28] N. Grzesiak, R. Blümel, K. Wright, K. M. Beck, N. C. Pisenti, M. Li, V. Chaplin, J. M. Amini, S. Debnath, J.-S. Chen, and Y. Nam, Efficient arbitrary simultaneously entangling gates on a trapped-ion quantum computer, Nat. Commun. **11**, 2963 (2020).
[29] K. Wang, J.-F. Yu, P. Wang, C. Luan, J.-N. Zhang, and K. Kim, Fast multi-qubit global-entangling gates without individual addressing of trapped ions, Quantum Sci. Technol. **7**, 044005 (2022).
[30] T. Manovitz, Y. Shapira, L. Gazit, N. Akerman, and R. Ozeri, Trapped-ion quantum computer with robust entangling gates and quantum coherent feedback, PRX Quantum **3**, 010347 (2022).
[31] A. Sørensen and K. Mølmer, Quantum computation with ions in thermal motion, Phys. Rev. Lett. **82**, 1971 (1999).
[32] A. Sørensen and K. Mølmer, Entanglement and quantum computation with ions in thermal motion, Phys. Rev. A **62**, 022311 (2000).
[33] D. F. V. James, Quantum dynamics of cold trapped ions with application to quantum computation, Appl. Phys. B **66**, 181 (1998).
[34] Y. Shapira, R. Shaniv, T. Manovitz, N. Akerman, and R. Ozeri, Robust entanglement gates for trapped-ion qubits, Phys. Rev. Lett. **121**, 180502 (2018).
[35] J. Markov, Y. Shapira, N. Akerman, and R. Ozeri, Digital predistortion of optical field of a fast and high-fidelity entangling gate for trapped ions qubits, in *54th Annual Meeting of the APS Division of Atomic, Molecular and Optical Physics* (2023), https://meetings.aps.org/Meeting/DAMOP23/Session/U09.2.
[36] See Supplemental Material at http://link.aps.org/supplemental/10.1103/PhysRevLett.134.010602 for technical derivation and fitting details.
[37] H. F. Trotter, On the product of semi-groups of operators, Proc. Am. Math. Soc. **10**, 545 (1959).
[38] M. Suzuki, Generalized Trotter's formula and systematic approximants of exponential operators and inner derivations with applications to many-body problems, Commun. Math. Phys. **51**, 183 (1976).
[39] L. Peleg, N. Akerman, T. Manovitz, M. Alon, and R. Ozeri, Phase stability transfer across the optical domain using a commercial optical frequency comb system, arXiv:1905.05065.
[40] R. Shankar, Exact solution of the two–dimensional ising model, in *Quantum Field Theory and Condensed Matter: An Introduction* (Cambridge University Press, Cambridge, England, 2017), pp. 114–142, 10.1017/9781139044349.009.
[41] Y. I. M. Büttiker and R. Landauer, Josephson behavior in small normal one-dimensional rings, Phys. Lett. A **96**, 365 (1983).
[42] H.-F. Cheung, Y. Gefen, E. K. Riedel, and W.-H. Shih, Persistent currents in small one-dimensional metal rings, Phys. Rev. B **37**, 6050 (1988).
[43] A. Kyprianidis, A. J. Rasmusson, and P. Richerme, Interaction graph engineering in trapped-ion quantum simulators with global drives, New J. Phys. **26**, 023033 (2024).
[44] M. Li, N. H. Nguyen, A. M. Green, J. Amini, N. M. Linke, and Y. Nam, Realizing two-qubit gates through mode engineering on a trapped-ion quantum computer, arXiv:2208.01584.
[45] J. D. Arias Espinoza, M. Mazzanti, K. Fouka, R. X. Schüssler, Z. Wu, P. Corboz, R. Gerritsma, and A. Safavi-Naini, Engineering spin-spin interactions with optical tweezers in trapped ions, Phys. Rev. A **104**, 013302 (2021).
[46] C. E. Granade, C. Ferrie, N. Wiebe, and D. G. Cory, Robust online Hamiltonian learning, New J. Phys. **14**, 103013 (2012).
[47] E. Bairey, I. Arad, and N. H. Lindner, Learning a local Hamiltonian from local measurements, Phys. Rev. Lett. **122**, 020504 (2019).
[48] E. Ben Av, Y. Shapira, N. Akerman, and R. Ozeri, Direct reconstruction of the quantum-master-equation dynamics of a trapped-ion qubit, Phys. Rev. A **101**, 062305 (2020).

[49] S. A. Guo, Y. K. Wu, J. Ye, L. Zhang, Y. Wang, W. Q. Lian, R. Yao, Y. L. Xu, C. Zhang, Y. Z. Xu, B. X. Qi, P. Y. Hou, L. He, Z. C. Zhou, and L. M. Duan, Hamiltonian learning for 300 trapped ion qubits with long-range couplings, arXiv:2408.03801.

[50] R. Shaniv, T. Manovitz, Y. Shapira, N. Akerman, and R. Ozeri, Toward Heisenberg-limited Rabi spectroscopy, Phys. Rev. Lett. **120**, 243603 (2018).

[51] R. Shaniv, N. Akerman, T. Manovitz, Y. Shapira, and R. Ozeri, Quadrupole shift cancellation using dynamic decoupling, Phys. Rev. Lett. **122**, 223204 (2019).

[52] T. Manovitz, R. Shaniv, Y. Shapira, R. Ozeri, and N. Akerman, Precision measurement of atomic isotope shifts using a two-isotope entangled state, Phys. Rev. Lett. **123**, 203001 (2019).